CHAPTER 5
LIMITATIONS

5.1 Introduction

The quality of a first order diffraction tomographic reconstruction is limited by both mathematical approximations and experimental limitations. In the derivation of a model for the scattered fields either the Born or the Rytov approximation is used to solve the integral equations for the scattered field. These approximations are a source of error and limit the types of objects that can be imaged with diffraction tomography. The only way to reduce this type of error is to use a better model or a higher order approximation. Better models for the scattered field will be discussed in Chapter 6.

The experimental limitations, on the other hand, are caused by a shortage of data. It is only possible to collect a finite amount of data about the scattered field and the experimental errors can be attributed to interpolation errors, aliasing and the finite aperture. Up to the limit in resolution caused by evanescent waves and the limit in quality due to the Born and the Rytov approximations it is possible to improve a reconstruction by collecting additional data.

Computer simulations are presented in this chapter illustrating the errors in first order diffraction tomography. To study the effects of the Born and the Rytov approximations it is necessary to calculate (or even measure) the exact scattered fields and then use the most accurate reconstruction algorithms available. The experimental errors can be minimized by calculating a large number of data points and using a circularly symmetric object to reduce the errors due to angular sampling. If experimental errors are minimized then the only remaining source of errors are caused by the approximations made in the reconstruction algorithm. As already mentioned the mathematical limitations on the reconstructions are a function of the object's size and refractive index.

The experimental errors are highlighted by minimizing the algorithmic errors. This can be done in two ways. The more straightforward method is to choose a small object with a small change in refractive index. As the size of the object and its refractive index are reduced both the Born and the Rytov

approximations more accurately model the exact scattered field. A second approach is to assume the Born or Rytov approximations are valid then use the Fourier Diffraction Theorem to generate the scattered fields from the Fourier transform of the object. In both cases the amount of data calculated is varied to highlight the different experimental errors.

5.2 Mathematical Limitations

In diffraction tomography there are different approximations involved in the forward and inverse directions. In the forward process it is necessary to assume that the object is weakly scattering so that either the Born or the Rytov approximations can be used. Once an expression for the scattered field is derived it is necessary to not only to measure the scattered fields but then numerically implement the inversion process.

To study the limits of the mathematical approximations the exact field for the scattered field from a cylinder as shown by Weeks [Wee64] and by Morse and Ingard [Mor68] is calculated for cylinders of various sizes and refractive index. In the simulations that follow a single plane wave of unit wavelength is incident on the cylinder and the scattered field is measured along a line at a distance of 100 wavelengths from the origin. In addition all refractive index changes are modeled as monopole (omnidirectional) scatterers. By doing this the directional dependence of dipole scatterers does not have to be taken into account.

At the receiver line the received wave is measured at 512 points spaced at 1/2 wavelength intervals. In all cases the rotational symmetry of a single cylinder at the origin is used to reduce the computation time of the simulations. Since all projections are identical this eliminates any angular interpolation error.

5.2.1 Evaluation of the Born Approximation

In using the Born approximation it is necessary to assume that the amplitude of the scattered field is small compared to the incident field. As already discussed the Born approximation is most sensitive to phase changes and this will be shown, first qualitatively and then quantitatively. From Chapter 2 the phase change is given by

$$\text{Phase Change} = 4\pi n_\delta \frac{a}{\lambda} \tag{5.1}$$

where the cylinder has a radius of 'a' and a refractive index of $1+n_\delta$.

The results shown in Figure 5.1 are for cylinders of four different refractive indices. In addition Figure 5.2 shows plots of each reconstruction along a line through the center of the cylinder. Notice that the y coordinate (refractive index) of the center line is plotted in terms of change from unity.

Simulations are shown for refractive indices that range from .1% change (refractive index of 1.001) to a 40% change (refractive index of 1.4). For each refractive index, cylinders of size 1, 2, 4 and 10 wavelengths are shown. This gives a range of phase changes across the cylinder (see equation (5.1) above) from $.004\pi$ to 16π.

Clearly, all the cylinders of refractive index 1.001 in Figure 5.1 are perfectly reconstructed. As equation (5.1) predicts the results get worse as the product of refractive index and radius gets larger. The largest refractive index that is successfully reconstructed is for the cylinder in Figure 5.1 of radius 1 wavelength and a refractive index that differed by 20% from the surrounding medium.

While it is difficult to evaluate quantitatively the three dimensional plots it is certainly reasonable to conclude that only cylinders where the phase change across the object is less than or equal to $.8\pi$ are adequately reconstructed. In general the reconstruction for each cylinder where the phase change across the cylinder is greater than π shows severe artifacts near the center. This limitation in the phase change across the cylinder is consistent with the condition described in Chapter 2.

5.2.2 Evaluation of the Rytov Approximation

Figure 5.3 shows the simulated results for 16 reconstructions using the Rytov approximation. To emphasize the insensitivity of the Rytov approximation to large objects the largest object simulated has a diameter of 100λ.

It should be pointed out that the rounded edges of the 1λ reconstructions are not due to any limitation of the Rytov approximation but instead are the result of a two dimensional low pass filtering of the reconstructions. Recall that for a transmission experiment an estimate of the object's Fourier transform is only available up to frequencies less than $\sqrt{2}k_0$. Thus the reconstructions shown in Figure 5.3 show the limitations of both the Rytov approximation and the Fourier Diffraction Theorem.

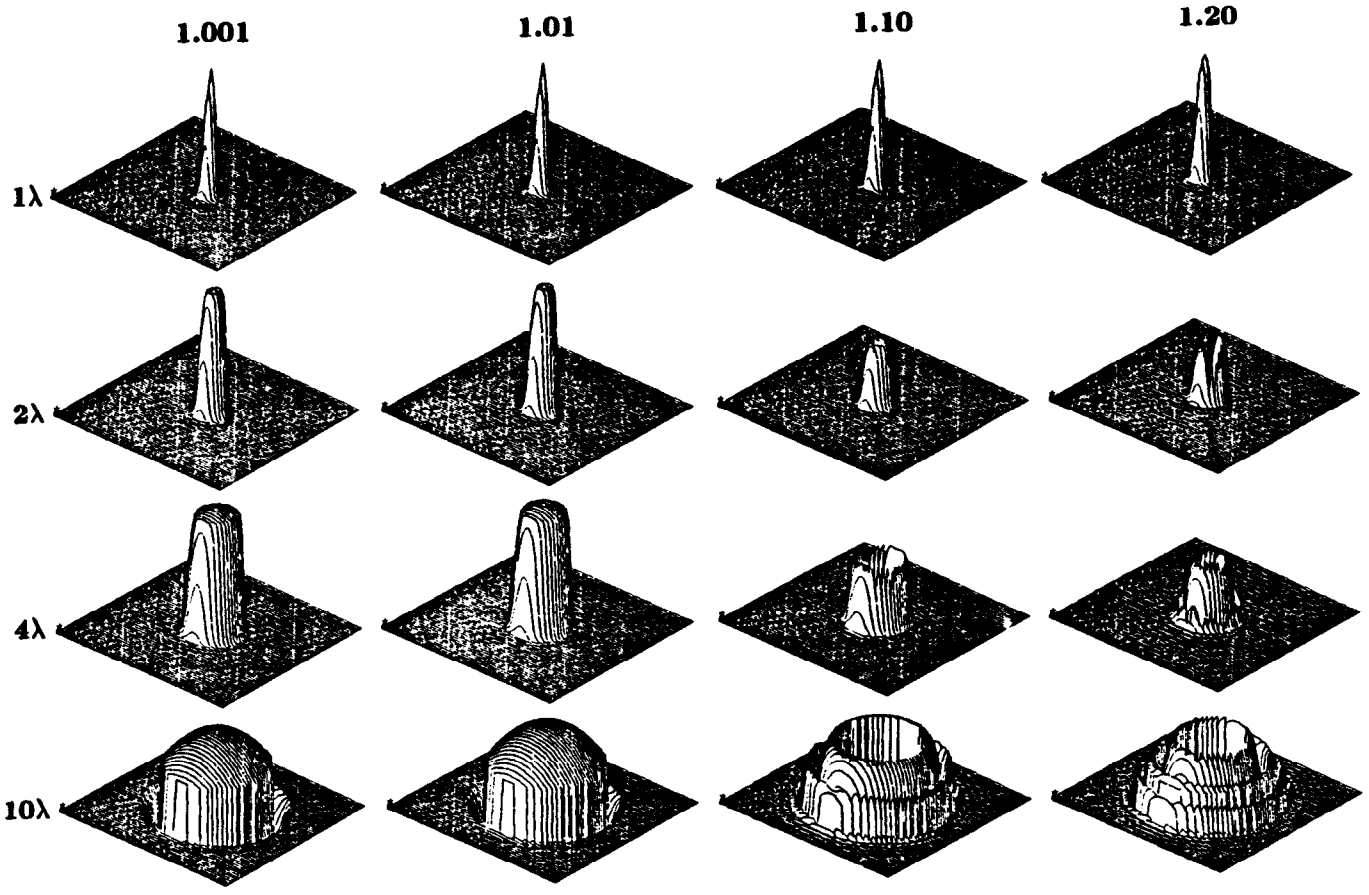

Figure 5.1 Simulated reconstructions using the Born approximation for 16 objects with four refractive indices between 1.001 and 1.20 and four radii between 1 and 10λ.

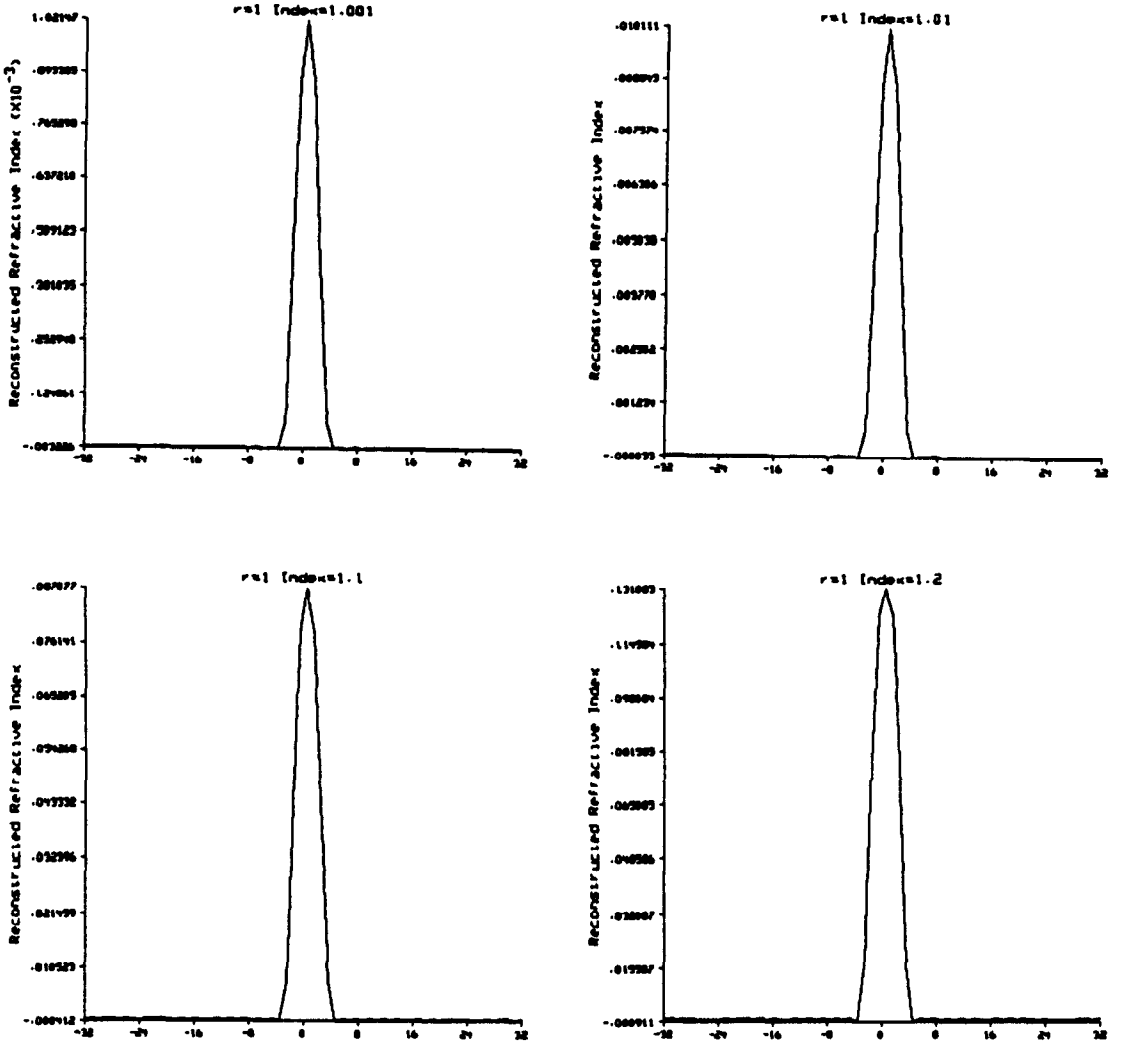

Figure 5.2 The center line for the reconstructions shown in Figure 5.1.

5.2.3 Comparison of the Born and Rytov Approximation

Reconstructions using exact scattered data show the similarity of the Born and the Rytov approximation. Within the limits of the Fourier Diffraction Theorem the reconstructions in Figure 5.1 and 5.3 of a 1λ object with a small refractive index are similar. In both cases the reconstructed change in refractive index is close to that of the simulated object.

The two approximations differ for objects that have a large refractive index change or have a large radius. The Born reconstructions are good at a large refractive index as long as the phase shift of the incident field as predicted by equation (5.1) is less than π.

On the other hand the Rytov approximation is very sensitive to the refractive index but produce excellent reconstructions for objects as large as 100λ. Unfortunately for object with a refractive index larger than 1% the Rytov approximation quickly deteriorates.

In addition to the qualitative studies a quantitative study of the error in the Born and Rytov reconstructions is also possible. As a measure of error the relative mean squared error in the reconstruction of the object function is integrated over the entire plane. If the actual object function is o(r) and the reconstructed object function is o′(r) then the relative Mean Squared Error (MSE) is given by

$$\frac{\int\int [o(r)-o'(r)]^2 dr}{\int\int [o(r)]^2}. \qquad (5.2)$$

This study presents the Mean Squared Error for 120 reconstructions based on the exact scattered fields from a cylinder. In each case a 512 point receiver line is at a distance of 10 λ from the center of the cylinder. Both the receiver line and the object reconstruction are sampled at 1/4 λ intervals.

The plots of Figure 5.4 present a summary of the mean squared error for cylinders of 1, 2 and 3 λ in radius and for twenty refractive indices between 1.01 and 1.20. In each case the error for the Born approximation is shown as a solid line while the Rytov reconstruction is shown as a dashed line. The data used for these simulations was the exact scattered fields from a cylinder measured at 512 receiver points along a receiver line 10λ from the center of the cylinder.

Many researchers [Kav82, Kel69, Sou83] have postulated that the Rytov approximation is clearly superior to the Born but as the actual reconstructions represented by Figure 5.4 show for a 1λ cylinder this is not necessarily true. It

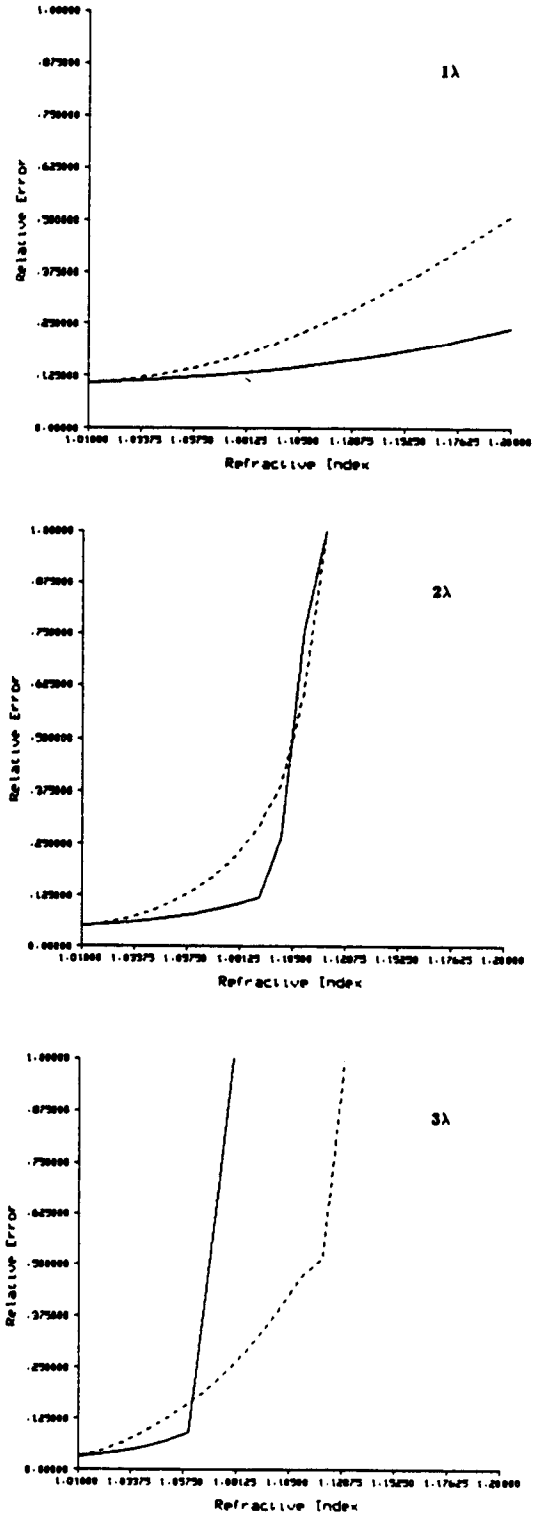

Figure 5.4 The relative mean squared error for reconstructions using the Born (solid line) and Rytov (dashed line) approximations. The error for a total of 60 objects with a radius of 1, 2 and 3 wavelengths are shown.

is interesting to note that, while the Rytov approximation shows a steadily increasing error with higher refractive indices, the error in the Born reconstruction is relatively constant until a threshold is reached. For the 2λ and 3λ cylinders, this breakpoint occurs at a phase shift across the cylinder of 0.6 and 0.7π. Thus, a criteria for the validity of the Born approximation is that the product of the radius of the cylinder in wavelengths and the change in refractive index must be less than .175.

Figure 5.5 presents a summary of the relative mean squared errors for cylinders with refractive indices of 1.01, 1.02 and 1.03 for forty radii between 1 and 40λ. Because the size of the cylinders varied by a factor of forty, the simulations parameters were adjusted accordingly. For a cylinder of radius R, the scattered field was calculated for 512 receivers along a line 2R from the center of the cylinder and spaced at 1/16R intervals.

In each of the simulations, the Born approximation is only slightly better than the Rytov approximation until the Born approximation crosses its threshold with a phase shift of 0.7π. Because the error in the Rytov approximation is relatively flat, it is clearly superior for large objects with small refractive indices. Using simulated data and the Rytov approximation objects as large as 2000λ in radius have been reconstructed.

5.3 Evaluation of Reconstruction Algorithms

To study the approximations involved in the reconstruction process it is necessary to calculate scattered data assuming the forward approximations are valid. This can be done in one of two different ways. As already discussed the Born and Rytov approximations are valid for small objects and small changes in refractive index. Thus, if the exact scattered field for a small and weakly scattering object is calculated then it can be assumed that either the Born or the Rytov approximations is exact.

A better approach is to recall the Fourier Diffraction Theorem, which says that the Fourier transform of the scattered field is proportional to the Fourier transform of the object along a circular arc. Since this theorem is the basis for the first order inversion algorithms if it is assumed correct the approximations involved in the reconstruction process can be studied.

If the Fourier Diffraction Theorem holds, the exact scattered field can be calculated exactly for objects that can be modeled as ellipses. The analytic expression for the Fourier transform of the object along an arc is then proportional to the scattered fields. This procedure is fast and allows the

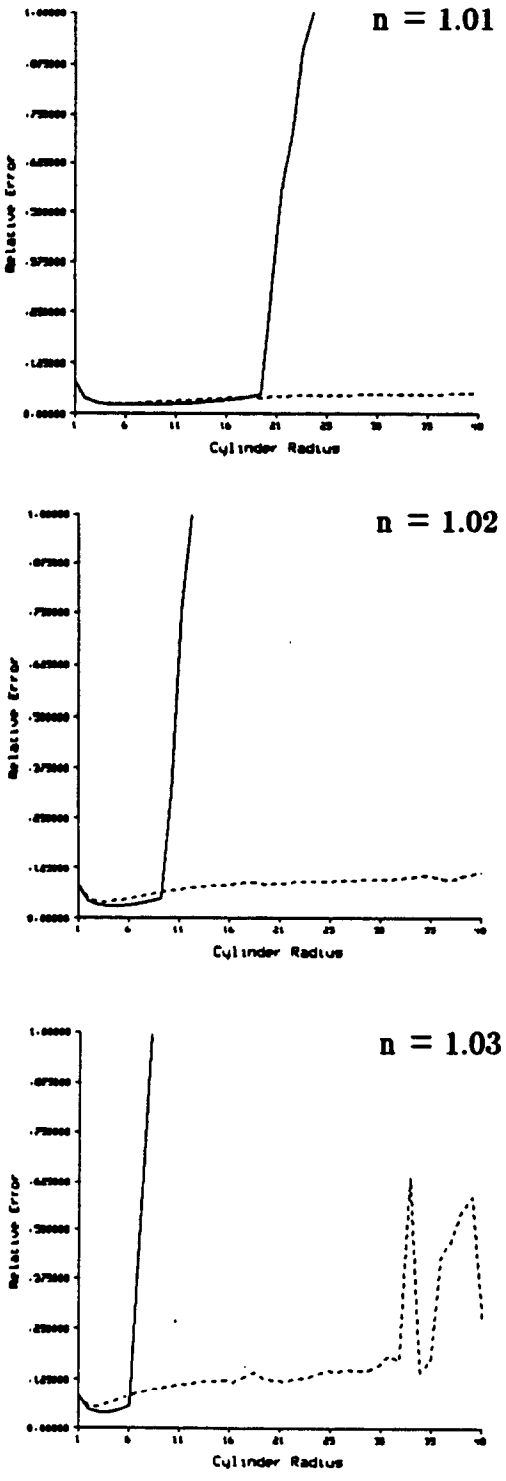

Figure 5.5 The relative mean squared error for reconstructions using the Born (solid line) and Rytov (dashed line) approximations. The error for a total of 120 objects with a refractive index of 1.01, 1.02 and 1.03 are shown.

scattered fields to be calculated for testing reconstruction algorithms and experimental parameters.

To illustrate the accuracy of the interpolation based algorithms, the image in Figure 5.6a will be used as a test "object" for showing computer simulation results. Figure 5.6a, with its gray levels as shown in Figure 5.6b, is a modification of the Shepp and Logan "phantom" described in [She74] to the case of diffraction imaging [Dev83, Pan83]. The gray levels shown in Figure 5.6 represent the refractive index values. This test image is a superposition of ellipses, with each ellipse being assigned a refractive index value as shown in Table 5.1.

Table 5.1. Summary of parameters for diffraction tomography simulations

Center Coordinate	Major Axis	Minor Axis	Rotation Angle	Refractive Index
(0,0)	0.92	0.69	90	1.0
(0,-0.0184)	0.874	0.6624	90	-0.5
(0.22,0)	0.31	0.11	72	-0.2
(-0.22,0)	0.41	0.16	108	-0.2
(0,0.35)	0.25	0.21	90	0.1
(0,0.1)	0.046	0.046	0	0.15
(0,-0.1)	0.046	0.046	0	0.15
(-0.08,-0.605)	0.046	0.023	0	0.15
(0,-0.605)	0.023	0.023	0	0.15
(0.06,-0.605)	0.046	0.023	90	0.15

A major advantage of using an image like Figure 5.6a for computer simulation is that the analytical expressions for the transforms of the diffracted projections can be written. The Fourier transform of an ellipse of semi-major and semi-minor axes A and B, respectively, is given by

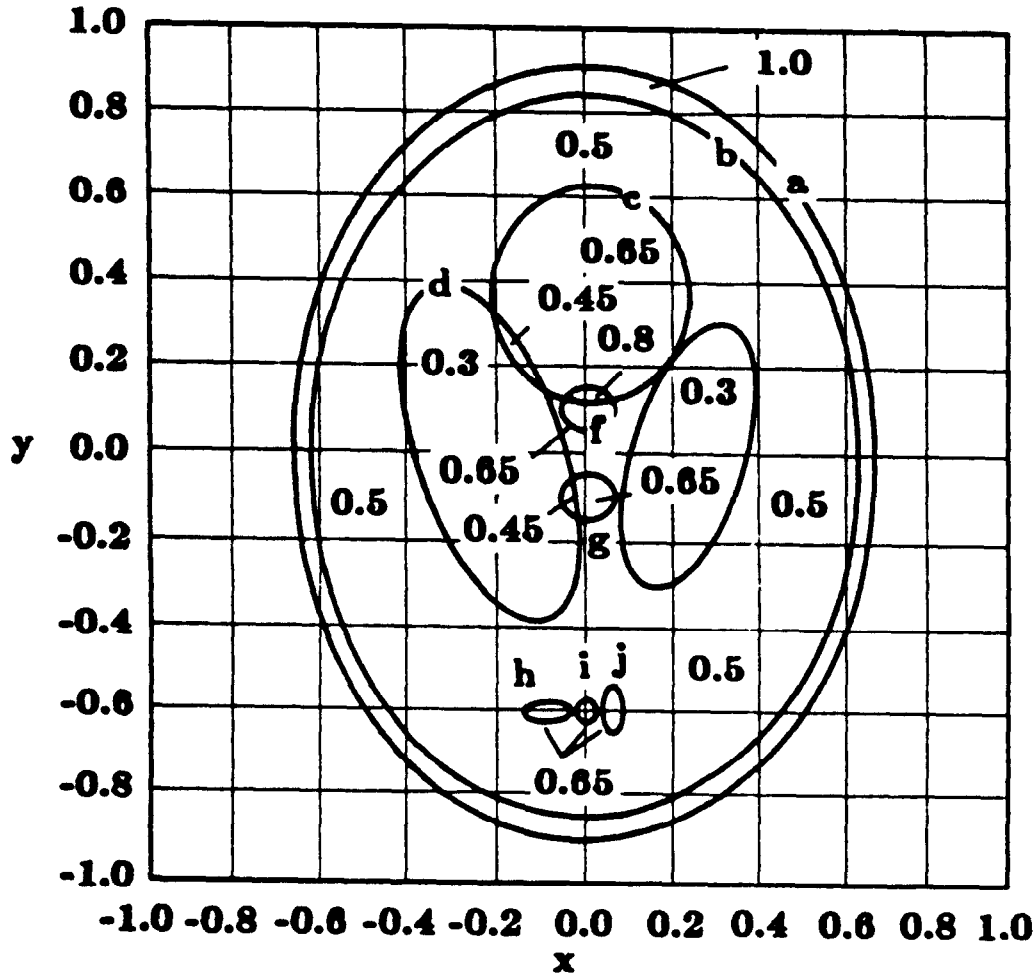

Figure 5.6 A modified version of the Shepp and Logan head phantom is used to test reconstruction algorithms. The numbers represent the relative change in refractive index from the background value of 1.0.

$$O_{ellipse}(u,v) = \frac{2\pi A J_1\left[B\sqrt{(uA/B)^2 + v^2}\right]}{\sqrt{(uA/B)^2 + v^2}} \tag{5.3}$$

where u and v are spatial angular frequencies in the x- and y-directions, respectively; and J_1 is a Bessel function of the first kind and order 1. When the center of this ellipse is shifted to the point (x_1,y_1), and the angle of the major axis tilted by α, as shown in Figure 5.7b, its Fourier transform becomes

$$e^{-j(ux_1+vy_1)} \cdot \frac{2\pi A J_1\left\{B\left[((u')A/B)^2 + (v')^2\right]^{1/2}\right\}}{\left[((u')A/B)^2 + (v')^2\right]^{1/2}} \tag{5.4}$$

where

$$u' = u\cos\alpha + v\sin\alpha \tag{5.5}$$

and

$$v' = -u\sin\alpha + v\cos\alpha. \tag{5.6}$$

Now consider the situation where the ellipse is illuminated by a plane. By the Fourier Diffraction Theorem the Fourier transform of the transmitted wave fields measured on the receiver line is given by the values of the above function on a circular arc. For the test object of Figure 5.7b, if weak scattering is assumed and therefore there is no interaction among the ellipses, the Fourier transform of the total forward scattered field measured on a line, is the sum of the values of functions like (5.4) over the circular arc. This procedure is used to generate the diffracted projection data for the test image.

It should be mentioned that by using this procedure to calculate the diffracted projection data only the accuracy of the reconstruction algorithm is tested, without checking whether or not the "test object" satisfies the underlying assumption of weak scattering. In order to test this crucial assumption, it is necessary to generate the forward scattered data of the object. For multi-component objects, such as the one shown in Figure 5.6a, it is very difficult to do so due to the interactions between the components.

Pan and Kak [Pan83] presented the simulations shown in Figure 5.8. Using a combination of increasing the sampling density by zero padding the signal and bilinear interpolation, results are obtained in 2 minutes of CPU time on a VAX 11/780 minicomputer with a floating point accelerator (FPA). The reconstruction is shown over a 128 by 128 grid using 64 views and 128 receiver positions. The number of operations required to carry out the interpolation

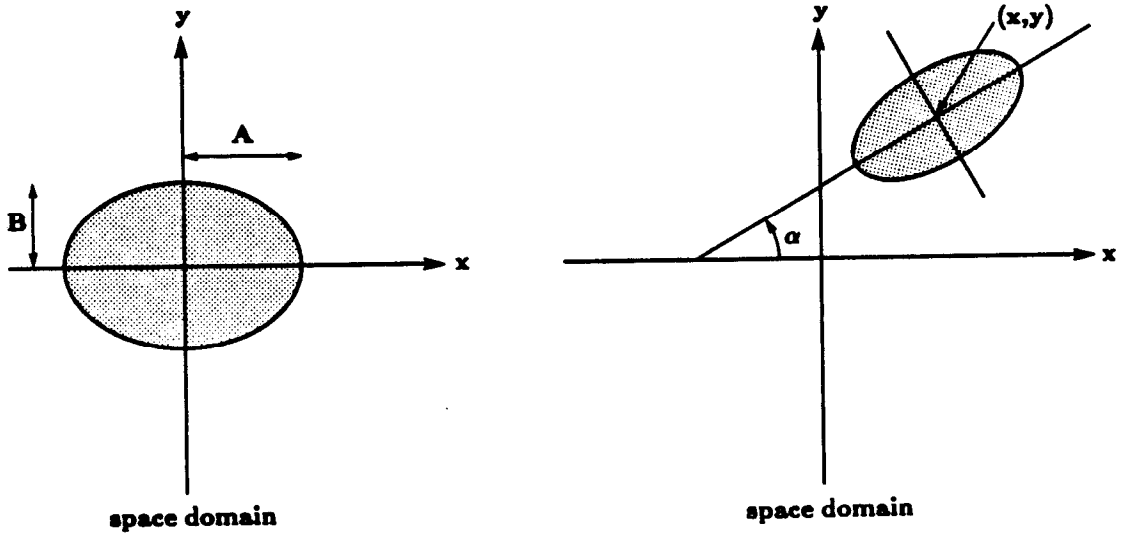

Figure 5.7 Assuming the Fourier Slice Theorem is valid the scattered field can easily be computed as the values of the Fourier transform of the rotated and translated ellipse.

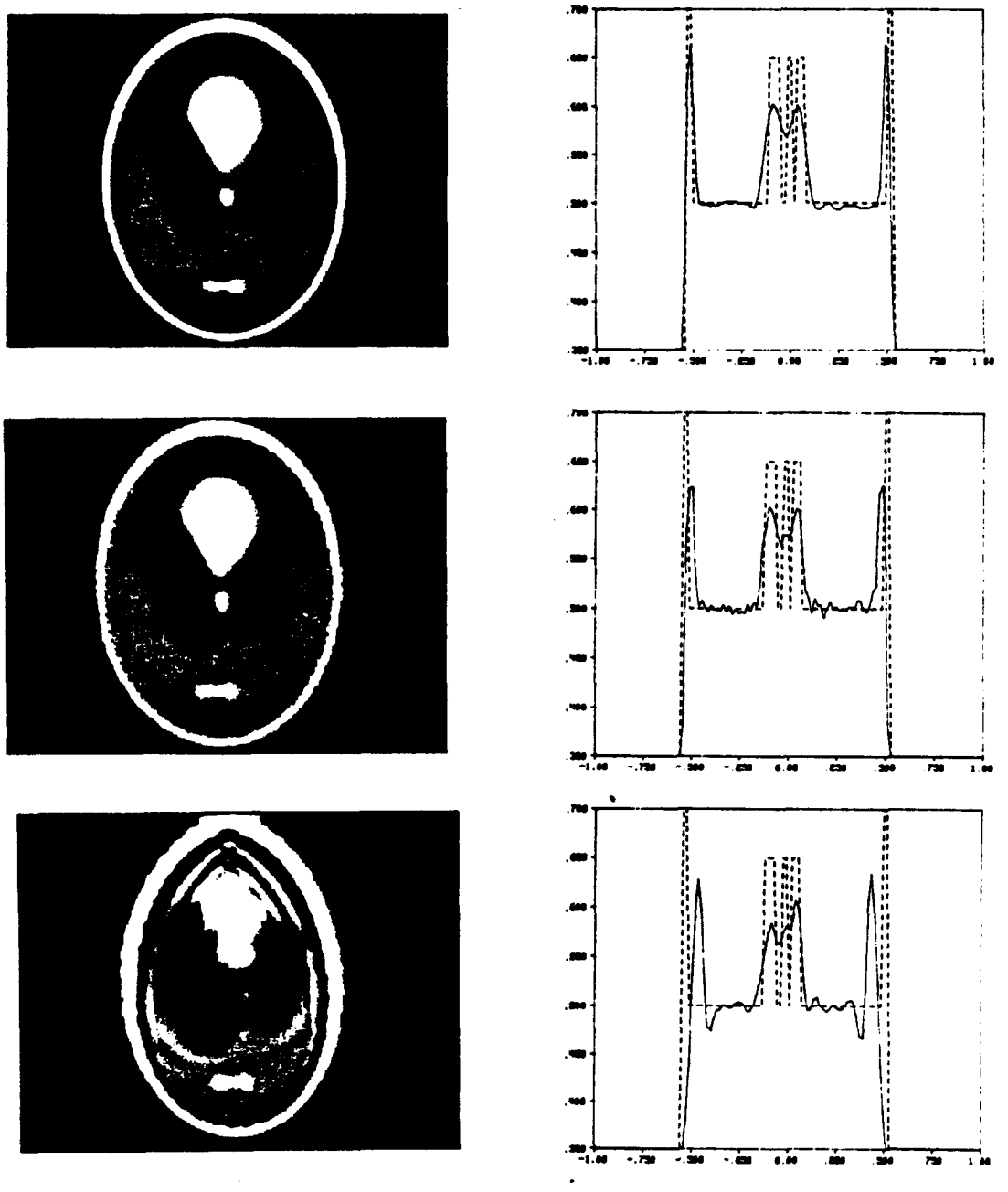

Figure 5.8 The above images show the results of using the (a) interpolation, (b) backpropagation and (c) modified backpropagation algorithms on reconstruction quality. The solid lines in the graphs represent the reconstructed value along a line through the center of the three ellipses at the bottom of the phantom.

and invert the object function is on the order of $N^2 \log N$. The resulting reconstruction is shown in Figure 5.8a.

Figure 5.8b represents the result of back propagating the data to 128 depths for each view while Figure 5.8c is the result of back propagation to only a single depth centered near the three small ellipses at the bottom of the picture. The results were calculated on a VAX 11/780 minicomputer with a Floating Point Accelerator (FPA) and the resulting reconstructions were done over a 128 by 128 grid. Like the previous image the input data consists of 64 projections of 128 points each.

There is a significant difference in not only the reconstruction time but also the resulting quality. While the modified back propagation only took 1.25 minutes the resulting reconstruction is much poorer than the full back propagation which took 30 minutes of CPU time. A comparison of the various algorithms is shown in Table 5.2.

Table 5.2. Comparison of Algorithms

Algorithm	Complexity	CPU Time
Interpolation	$N^2 \log N$	2 Minutes
Back Propagation	$N_d N_\phi N \log N$	30 Minutes
Modified Back Propagation	$N_\phi N \log N$	1.25 Minutes

5.4 Experimental Limitations

In addition to the limits on the reconstructions imposed by the Born and the Rytov approximations there are also experimental limitations. These additional factors are caused by

- Wave propagation in free space
- Sampling the data along the receiver line
- Finite receiver length
- Limited views of the object

In inverse scattering theory the measured complex amplitude of a received wave is sampled, filtered and then interpolated to estimate the Fourier transform of the object function. The reconstruction process is linear because

it consists only of filtering the data and then calculating its inverse Fourier transform.

The first three factors each can be modeled as a simple constant low-pass filtering of the scattered field. Because the entire process is linear the net effect is a single low filter at the lowest of the three frequencies. The experiment can be optimized by adjusting the parameters of the experiment so that each low pass filter cuts off at the same frequency.

A limited number of views also can be modeled as a low pass filter. In this case, though, the cutoff frequency varies with the radial direction.

5.4.1 Evanescent Waves

The most fundamental limitation is that evanescent waves are ignored. Since these waves have a complex wavenumber they are severely attenuated over a distance as small as several wavelengths. This limits the highest received wavenumber to

$$k_{max} = \frac{2\pi}{\lambda}. \tag{5.7}$$

This is a fundamental limit of the propagation process and the resolution of the reconstruction can only be improved by moving the experiment to a higher frequency (or shorter wavelength.)

5.4.2 Sampling the Received Wave

After the wave has been scattered by the object and propagated to the receiver line it must be measured. This is usually done with the a point receiver. Unfortunately it is not possible to sample at every point, so a non zero sampling interval must be chosen. This introduces a measurement error into the process. By the Nyquist theorem this can be modeled as a low pass filtering operation, where the highest measured frequency is given by

$$k_{meas} = \frac{\pi}{T} \tag{5.8}$$

and T is the sampling interval. Of course this analysis has ignored the non-linear effects of aliasing and the resulting frequency shifts that occur.

5.4.3 The Effects of a Finite Receiver Length

Not only are there physical limitations on the finest sampling interval but usually there is a limitation on the amount of data that can be collected. This generally means that samples of the received waveform will be collected at only a finite number of points along the receiver line. This is usually justified by taking data along a line long enough so that the unmeasured data can be safely ignored. Because of the wave propagation process this also introduces a low pass filtering of the received data.

Consider for a moment a single scatterer at some distance, l_0, from the receiver line. The wave propagating from this single scatterer is a cylindrical wave in two dimensions or a spherical wave in three dimensions. This effect is diagramed in Figure 5.9. It is easy to see that the spatial frequencies vary with the position along the receiver line.

An optician studying this problem would be interested in knowing the resolving power of the system as a function of the size of the aperture [Goo68]. The analysis would normally be carried out assuming that the object is far enough from the aperture so that it can be assumed it is in the aperture's far field. But in this work the frequency content of the measured field is a limiting factor in the reconstruction quality so the effect of a limited aperture will be analyzed with an emphasis on the spatial frequency content of the received field. The two approaches to be considered here use a point source and analyze the frequency content at the aperture. Since all points in space are in the far field of a point source this analysis gives identical results to classical optics theory.

It is easier to analyze the effect by considering the expanding wave to be locally planar at any point distant from the scatterer. At the point on the receiver line closest to the scatterer there is no spatial variation [Goo68]. This corresponds to receiving a plane wave or a received spatial frequency of zero.

Higher spatial frequencies are received at points along the receiver line that are farther from the origin. The received frequency is a function of the sine of the angle between the direction of propagation and a perpendicular to the receiver line. This function is given by

$$k(y) = k_{max}\sin\theta \tag{5.9}$$

where θ is the angle and k_{max} is the wavenumber of the incident wave. Thus at the origin, the angle, θ, is zero and the received frequency is zero. Only at infinity does the angle become equal to ninety degrees and the received spatial frequency approach the theoretical maximum.

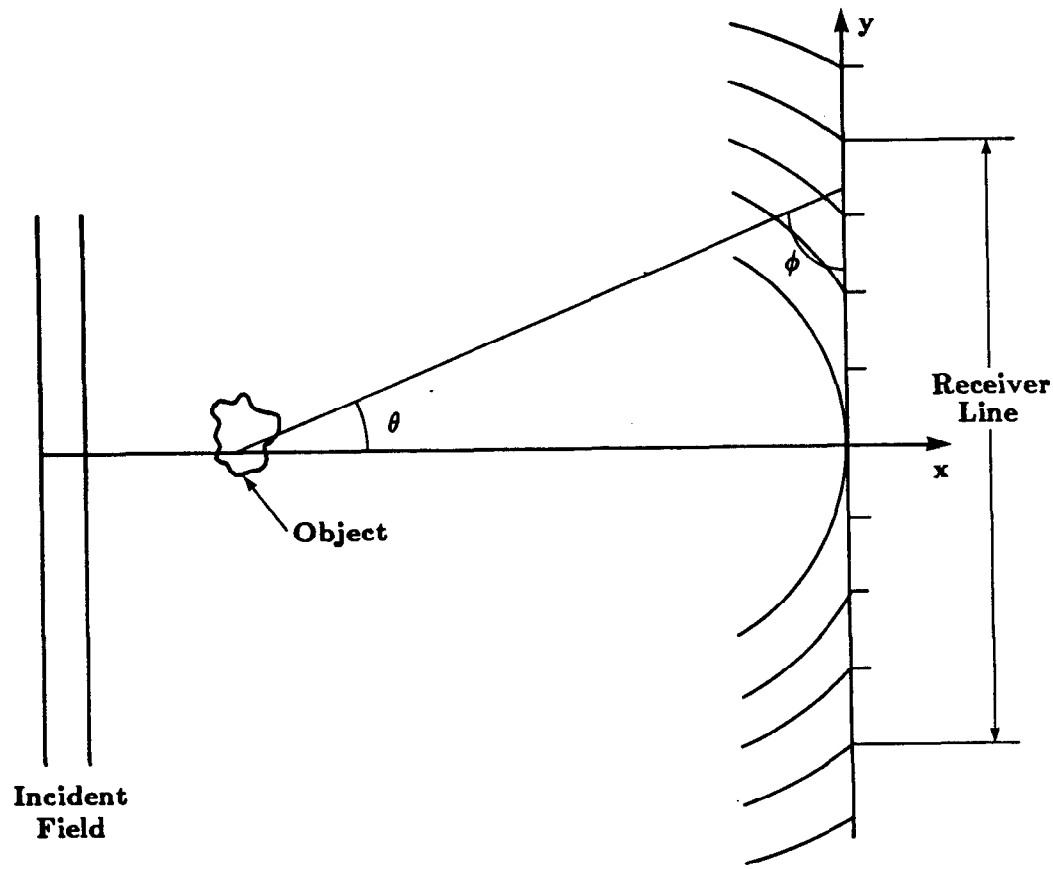

Figure 5.9 The field scattered by an object is measured along a receiver line with finite length.

This reasoning can be justified on a more theoretical basis by considering the phase of the propagating wave. The received wave at a point $(x=l_0,y)$ due to a scatterer at the origin is given by

$$u(x=l_0,y) = \frac{e^{jk_0\sqrt{x^2+y^2}}}{\sqrt{x^2+y^2}}. \tag{5.10}$$

The instantaneous spatial frequency along the receiver line (y varies) of this wave can be found by taking the partial derivative of the phase with respect to y [Gag78]

$$\text{phase} = k_0\sqrt{y^2+x^2} \tag{5.11}$$

$$k_{recv} = \frac{k_0 y}{\sqrt{x^2+y^2}} \tag{5.12}$$

where k_{recv} is the spatial frequency received at the point $(x=l_0,y)$. From Figure 5.9 it is easy to see that

$$\sin\theta = \frac{y}{\sqrt{x^2+y^2}} \tag{5.13}$$

and therefore equation (5.9) and (5.12) are equivalent.

This relation, (5.12), can be inverted to give the length of the receiver line for a given maximum received frequency, k_{max}. This becomes

$$y = \pm\frac{k_{max}x}{\sqrt{k_0^2-k_{max}^2}}. \tag{5.14}$$

Since the highest received frequency is a monotonically increasing function of the length of the receiver line it is easy to see that by limiting the sampling of the received wave to a finite portion of the entire line that a low passed version of the entire scattered wave is measured. The highest measured frequency is a simple function of the distance of the receiver line from the scatterer and the length of measured data. This limitation can be better understood if the maximum received frequency is written as a function of the angle of view of the receiver line. Thus substituting

$$\tan(\theta) = \frac{y}{x} \tag{5.15}$$

it is easy to see that

$$k_{recv} = \frac{k_0 \frac{y}{x}}{\sqrt{\left[\frac{y}{x}\right]^2 + 1^2}} \tag{5.16}$$

and

$$k_{recv} = \frac{k_0 \tan\theta}{\sqrt{\tan^2\theta + 1}}. \tag{5.17}$$

Thus k_{recv} is a monotonically increasing function of the angle of view, θ. It is easy to see that the maximum received spatial frequency can be increased by either moving the receiver line closer to the object or by increasing the length of the receiver line.

5.4.4 Evaluation of the Experimental Effects

Exact scattered data is used to verify the optimum experimental values and the effect of a finite receiver length is shown in Figure 5.10. The spatial frequency content of a wave is found by taking the FFT of the sampled points along the receiver line and is compared to the theoretical result as predicted by the Fourier Transform of the object. The theory predicts that more of the high frequency components will be present as the length of the receiver line increases and this is confirmed by simulation.

While the above derivation only considered a single scatterer it is also approximately true for many scatterers collected at the origin. This is possible because the inverse reconstruction process is linear and each point in the object scatterers an independent cylindrical wave.

5.4.5 Optimization

Since each of these three factors is independent, their effect in the frequency domain can be found by simply multiplying each of their frequency responses together. As has been described above each of these effects can be modeled as a simple low-pass filter of the theoretical data so the combined effect is also a low pass filter but at the lowest frequency of the cut-off of the three effects.

First consider the effect of ignoring the evanescent waves. Since the maximum frequency of the received wave is limited by the propagation filter to

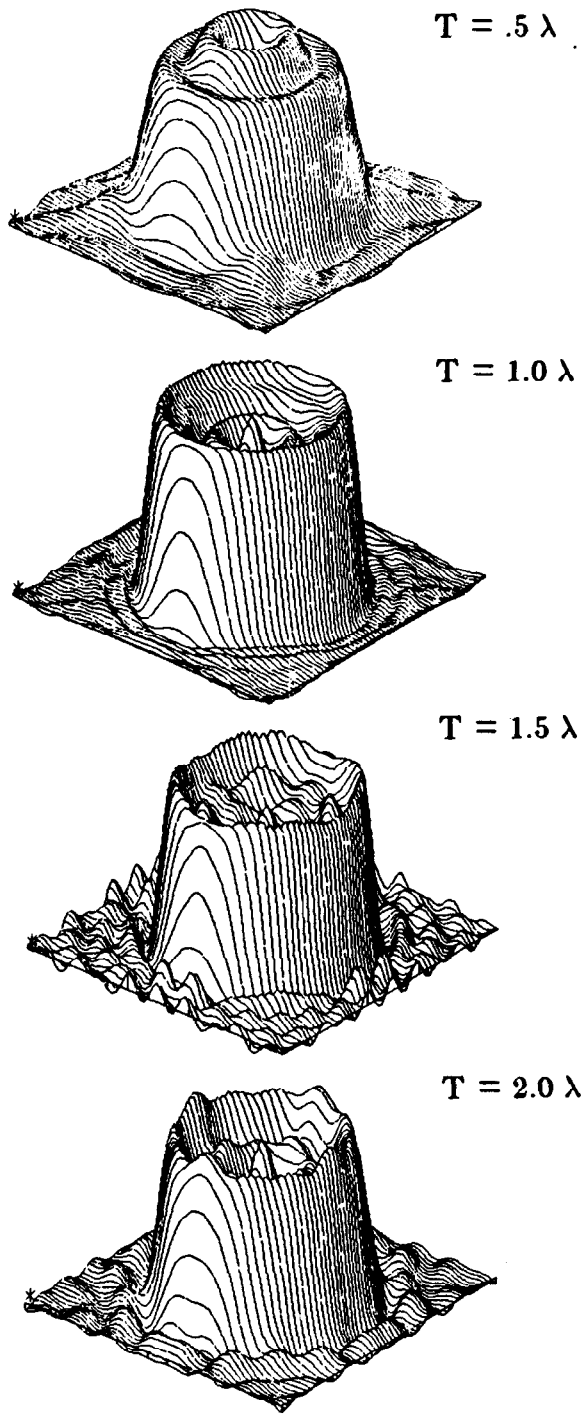

Figure 5.10 Reconstructions of an object using a detector spacing of (a) .5λ, (b) 1.0λ, (c) 1.5λ and (d) 2.0λ are shown here.

$$k_{max} = \frac{2\pi}{\lambda} \tag{5.18}$$

it is easy to combine this expression with the expression for the Nyquist frequency into a single expression for the smallest "interesting" sampling interval. This is given by

$$k_{max} = k_{meas} \tag{5.19}$$

or

$$\frac{2\pi}{\lambda} = \frac{\pi}{T} \tag{5.20}$$

and rearranging

$$T \geq 1/2\lambda. \tag{5.21}$$

Thus if the received waveform is sampled with a sampling interval of more than 1/2 wavelength the measured data might not be a good estimate of the received waveform because of aliasing. On the other hand it is not necessary to sample the received waveform any finer than 1/2 wavelength since this provides no additional information. Doing this it is possible to conclude that the sampling interval should be greater than 1/2 wavelength.

In general the experiment will also be constrained by the number of data points (M) that can be measured along the receiver line. The distance from the object to the receiver line will be considered a constant in the derivation that follows. If the received waveform is sampled uniformly, the range of the receiver line is given uniquely by

$$y_{max} = \pm\frac{MT}{2}. \tag{5.22}$$

This is also shown in Figure 5.9.

For a receiver line at a fixed distance from the object and a fixed number of receiver points this is a classical optimization problem. As the sampling interval is increased the length of the receiver line increases and more of the received wave's high frequencies are measured. On the other hand increasing the sampling interval lowers the maximum frequency that can be measured before aliasing occurs.

The optimum value of T can be found by setting the cutoff frequencies for the Nyquist frequency equal to the highest received frequency due to the finite receiver length and then solving for the sampling interval. If this constraint is not met then some of the information that is passed by one process will be attenuated by the others. This results in

$$\frac{\pi}{T} = \frac{k_0 y}{\sqrt{y^2+x^2}} \tag{5.23}$$

evaluated at

$$k_0 = \frac{2\pi}{\lambda} \tag{5.24}$$

and

$$y = \frac{MT}{2}. \tag{5.25}$$

Solving for T^2 the optimum value for T is given by

$$\left[\frac{T}{\lambda}\right]^2 = \frac{\sqrt{64\left[\frac{x}{\lambda}\right]^2 + M^2} + M}{8M}. \tag{5.26}$$

Making the substitution

$$\alpha = \frac{x}{\lambda M} \tag{5.27}$$

the optimum sampling interval is given by

$$\left[\frac{T}{\lambda}\right]^2 = \frac{\sqrt{64\alpha^2+1}+1}{8}. \tag{5.28}$$

This substitution is similar to the $\tan\theta$ substitution that is made in the heuristic approach above. Also notice that the smallest positive value that the sampling interval can become is 1/2 wavelength. This corresponds to the Nyquist frequency for a propagating wave.

The optimum sampling interval is confirmed by simulations. Again, using the method described above for calculating the exact scattered fields, four simulations are shown of an object of radius 10 wavelengths using a receiver that is 100 wavelengths from the object. In each case the number of receiver positions is fixed at 64. The resulting reconstructions for a sampling interval of .5, 1, 1.5 and 2 wavelengths are shown in Figure 5.10. Equation (5.28) predicts an optimum sampling interval of 1.3 wavelengths and this is confirmed by the simulations. The best reconstruction occurs with a sampling interval between 1 and 1.5 wavelengths.

5.4.6 Limited Views

In many applications it is not possible to generate or receive plane waves from all directions. The effect of this it to leave holes where there is no estimate of the Fourier transform of the object.

Since the ideal reconstruction algorithm produces an estimate of the Fourier transform of the object for all frequencies within a disk a limited number of views introduces a selective filter for areas where there is no data. As shown by Devaney [Dev84] for the VSP case a limited number of views degrades the reconstruction by low pass filtering the image in certain directions. Devaney's results are reproduced in Figures 5.11 and 5.12.

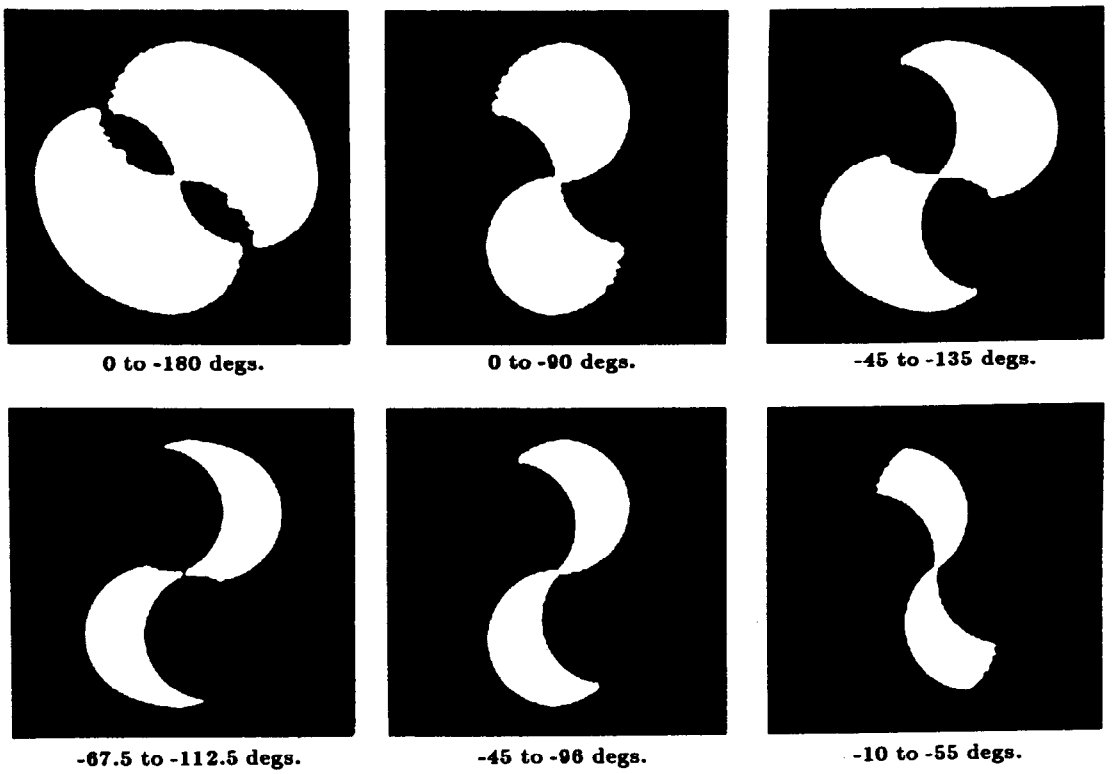

Figure 5.11 These figures show the coverage in the frequency domain for six different receiver limitations (from [Dev84]).

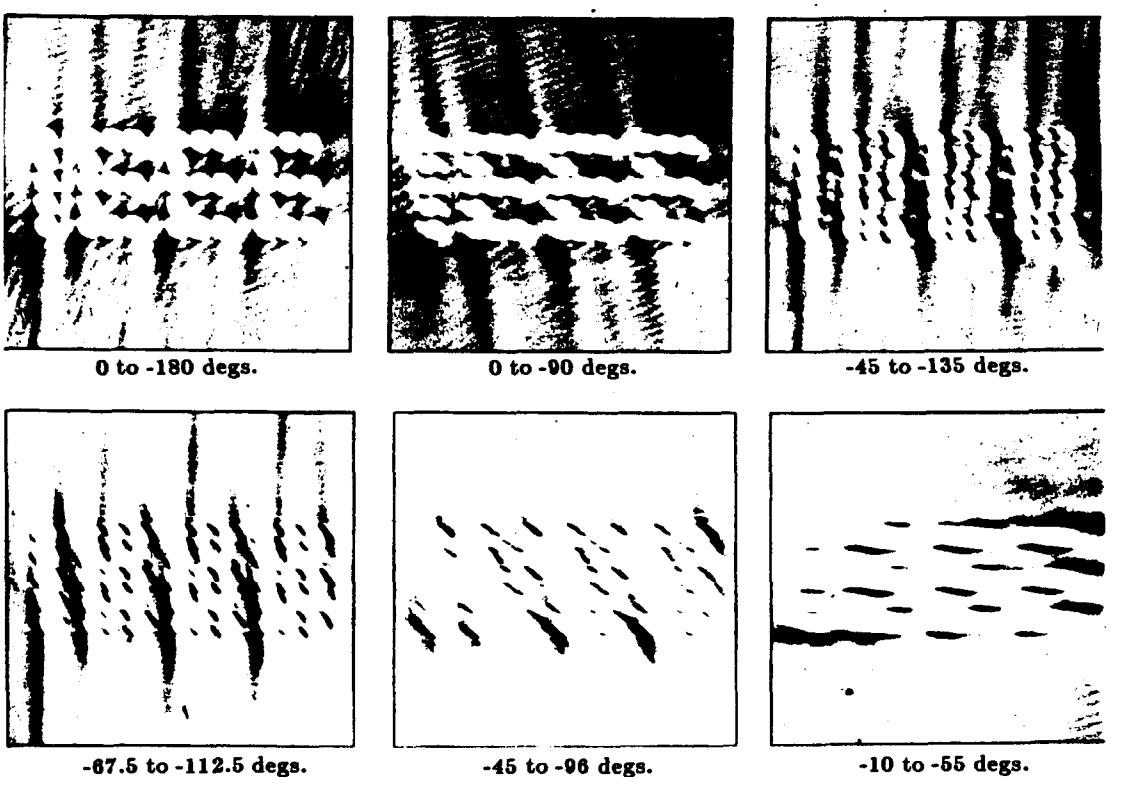

Figure 5.12 Images due to the limited field of views as shown in Figure 5.11 from [Dev84].

References

[Dev83] A. J. Devaney, "A computer simulation study of diffraction tomography," *IEEE Transactions on Biomedical Engineering,* Vol. BME-30, July 1983, pp. 377-386.

[Dev84] A. J. Devaney, "Geophysical diffraction tomography," *IEEE Transaction Geological Science, Special Issue on Remote Sensing,* Vol. GE-22, January 1984, pp. 3-13.

[Gag78] R. Gagliardi, *Introduction to Communications Engineering,* John Wiley and Sons, 1978.

[Goo68] J. W. Goodman, *Introduction to Fourier Optics,* McGraw Hill Book Company, San Francisco, 1968.

[Kav82] M. Kaveh, M. Soumekh, and R. K. Mueller, "Tomographic imaging via wave equation inversion," *ICASSP 82,* May 1982, pp. 1553-1556.

[Kel69] J. B. Keller, "Accuracy and validity of the Born and Rytov approximations," *Journal of the Optical Society of America,* Vol. 59, 1969, pp. 1003-1004.

[Mor68] P. M. Morse and K. U. Ingard, *Theoretical Acoustics,* McGraw Hill Book Company, New York, 1968.

[Pan83] S. X. Pan and A. C. Kak, "A computational study of reconstruction algorithms for diffraction tomography: Interpolation vs. filtered-backpropagation," *IEEE Transactions on Acoustics, Speech and Signal Processing,* October 1983, pp. 1262-1275.

[She74] L. A. Shepp and B. F. Logan, "The Fourier reconstruction of a head section," *IEEE Trans. Nucl. Sci.,* Vol. NS-21, 1974, pp. 21-43.

[Sou83] M. Soumekh, M. Kaveh, and R. K. Mueller, "Algorithms and experimental results in acoustic tomography using Rytov's approximation," *ICASSP 83 Proceedings,* April 1983, pp. 135-138.

[Wee64] W. L. Weeks, *Electromagnetic Theory for Engineering Applications,* John Wiley and Sons, Inc., New York, 1964.